ARL-TR-9267 ● AUG 2021

DEVCOM ARMY RESEARCH LABORATORY

3-D Microstructural Interface Characterization with In-situ X-Ray Micro-Computed Tomography Tensile Loading

by Jennifer M Sietins, Adam Taylor, Dave VanOosten, and Jason Robinette

NOTICES

Disclaimers

The findings in this report are not to be construed as an official Department of the Army position unless so designated by other authorized documents.

Citation of manufacturer's or trade names does not constitute an official endorsement or approval of the use thereof.

Destroy this report when it is no longer needed. Do not return it to the originator.

ARL-TR-9267 ● AUG 2021

3-D Microstructural Interface Characterization with In-situ X-Ray Micro-Computed Tomography Tensile Loading

Jennifer M Sietins, Dave VanOosten, and Jason Robinette
Weapons and Materials Research Directorate,
DEVCOM Army Research Laboratory

Adam Taylor
Drexel University

REPORT DOCUMENTATION PAGE			Form Approved OMB No. 0704-0188

1. REPORT DATE *(DD-MM-YYYY)*	2. REPORT TYPE	3. DATES COVERED (From - To)
August 2021	Technical Report	2018 May–2021 April

4. TITLE AND SUBTITLE	5a. CONTRACT NUMBER
3-D Microstructural Interface Characterization with In-situ X-Ray Micro-Computed Tomography Tensile Loading	5b. GRANT NUMBER
	5c. PROGRAM ELEMENT NUMBER
6. AUTHOR(S)	5d. PROJECT NUMBER
Jennifer M Sietins, Adam Taylor, Dave VanOosten, and Jason Robinette	5e. TASK NUMBER
	5f. WORK UNIT NUMBER

7. PERFORMING ORGANIZATION NAME(S) AND ADDRESS(ES)	8. PERFORMING ORGANIZATION REPORT NUMBER
DEVCOM Army Research Laboratory ATTN: FCDD-RLW-MB Aberdeen Proving Ground, MD 21005	ARL-TR-9267
9. SPONSORING/MONITORING AGENCY NAME(S) AND ADDRESS(ES)	10. SPONSOR/MONITOR'S ACRONYM(S)
	11. SPONSOR/MONITOR'S REPORT NUMBER(S)

12. DISTRIBUTION/AVAILABILITY STATEMENT

Approved for public release: distribution unlimited.

13. SUPPLEMENTARY NOTES

ORCID IDs: Jason Robinette, 0000-0003-4096-8502; Jennifer M Sietins, 0000-0003-2547-1653;
Adam Taylor, 0000-0003-1618-3270

14. ABSTRACT

Interfaces play a critical role in the resulting mechanical performance and failure mechanisms of composite materials; however, interface characterization can be challenging. This report summarizes an X-ray micro-computed tomography technique to quantitatively measure cavities between glass particles and a polyurea matrix during in-situ tensile loading. This material is a mock surrogate for energetic materials of interest with similar interfacial chemistry, particle loading, and size distribution. We believe the fundamental failure mechanisms will apply to similar energetic composites. Our work investigated glass particles with and without a silane coating scanned at both a low and high loading strain. Subsequent analysis quantified the number and magnitude of cavity separations, their volume, and the volume of each cavity's respective glass sphere. Results showed the coated particles had less frequent separations compared to the uncoated particles at both the low and high tensile strains. Unexpectedly, there was not a preferential cavity formation initiating on the larger glass volumes when comparing the cavity sizes to their respective glass sphere sizes. This experimental technique offers a unique opportunity to assess 3-D cavity formation and growth in particle-filled composite materials, which can provide an increased fundamental understanding of a composite interface's role during failure.

15. SUBJECT TERMS

X-ray micro-computed tomography, in-situ tensile testing, interface characterization, microstructural analysis, cavity quantification, surface treatment

16. SECURITY CLASSIFICATION OF:			17. LIMITATION OF ABSTRACT	18. NUMBER OF PAGES	19a. NAME OF RESPONSIBLE PERSON
a. REPORT	b. ABSTRACT	c. THIS PAGE			Jennifer M Sietins
Unclassified	Unclassified	Unclassified	UU	26	19b. TELEPHONE NUMBER (Include area code) (410) 306-1949

Standard Form 298 (Rev. 8/98)
Prescribed by ANSI Std. Z39.18

Contents

List of Figures

List of Tables

Acknowledgments

The authors would like to thank Dr Ian McAninch for his assistance conducting the particle size analysis that allowed independent confirmation of the hypothesized explanation.

1. Introduction

Particle composites are used extensively in many industries because adding particle fillers is relatively inexpensive and there is improved mechanical performance, including material toughening, strengthening, and stiffening. Part performance can be tailored based upon a number of factors including the materials, volume fractions of the fillers, particle shape and size, and if a surface functionalization treatment has been applied on the filler material to improve adhesion with the matrix. While particle-filled composites have been studied for quite some time, there is still a lack of understanding regarding composite interfaces and the ability to fully characterize them.

It is widely reported that the volume fraction, particle size, strain rate, and adhesion between the particle and matrix greatly influence interface debonding and therefore the composite's mechanical properties. In particular, the particle size has been reported as one of the primary factors for the debonding stress in particle-filled composites[1]; however, that is primarily for particles that are not chemically bonded to the matrix. Others have reported only minor changes of little or no significance based upon changes in the glass bead size.[2–4] The particle size has been found to be of secondary importance compared to the overall volume fraction (or solids loading), which is much more dominant.[2]

Understanding the drivers of mechanical strength in particle composites is crucial to ongoing research in energetic applications such as propellant. In the interest of next-generation munitions, elastomeric polymers, desired for their toughness, are being optimized for solids loading. To outperform currently fielded munitions, the propellant must contain a volume share of energetic particles approaching the maximum packing fraction. However, to achieve a consistent projectile launch profile from shot to shot the material must remain cohesive under the violent stresses of ballistic firing. For these materials to be successful, the ability to study the adhesion and failure mechanisms in-situ with regard to particle size, shape, and quantity would be greatly advantageous.

There are significant challenges to measuring the debonding between particles and matrix during in-situ loading. Prior experimental methods used optical or scanning electron microscopy to observe the extent of particle separations and compared coated and uncoated specimens.[5–7] These methods, however, only image the debonding of particles visible on the outer surfaces of the sample and do not account for all of the internal separations that may be occurring. Additionally, most of these morphological observations are conducted on the fracture surfaces of failed

specimens, which does not account for the larger cavity sizes during loading as elastic matrices begin to relax after tensile loading is released.

X-ray micro-computed tomography (XCT) is a 3-D imaging technique that captures thousands of projection images and reconstructs those images into a full 3-D volume that can be virtually sliced in any direction. Materials of different densities appear with different grayscale contrasts and can be segmented for further visualizations or quantitative analysis. XCT imaging during in-situ mechanical testing has shown global deformations, crack initiation and propagations, void nucleation and growth, and fiber reorientation to align with the direction of tensile loading. An extensive amount of work in this area involved synchrotrons, due to their high-intensity flux and high-resolution imaging. Babout et al. performed a similar study to this work and successfully imaged decohesion and cavity growth in a metal matrix composite rather than a polymer matrix composite using a synchrotron.[8] Advancements in laboratory scanners allow high-resolution XCT imaging and the incorporation of in-situ loading stages, but the scan times are significantly longer than the synchrotrons.[9]

This report summarizes a technique to quantify cavity formation and growth in a particle-filled polymer matrix composite using laboratory XCT to obtain data that characterizes the internal microstructure in all three dimensions. The debonding between the interface of glass particles and the matrix were studied at low and high strains and with samples that included a silane coating for improved adhesion. More advanced segmentation and analysis algorithms were employed to classify glass spheres with and without attached cavities to draw conclusions regarding any preferential formation of cavities based on the size of their respective glass spheres.

2. Procedure

2.1 Sample Preparation

An energetic simulant of Ebecryl 230 urethane acrylate (UA)/isobornyl acrylate (IBA) (60/40 wt%) was mixed with a filler of Potters Spheriglass microspheres of 60–70 μm diameter (2530 grade). Uncoated and silane-coated beads were used as received from Potters Industries, LLC. The filler ratio was 10 vol% solids loading. The mixtures were poured into a 55-mL mold that was 12.7 × 12.7 × 0.3 cm with a steel back plate and gasket around the edges. The mold was topped with a glass plate and UV cured at 400 W with a metal halide bulb. After curing, the samples were removed from the mold and machined to a tensile dog-bone shape approximately 10.5 mm in height as illustrated in Fig. 1.

Fig. 1 Sample geometry prior to tensile testing

2.2 X-ray Micro-Computed Tomography (XCT)

The US Army Combat Capabilities Development Command Army Research Laboratory has two XCT systems with accompanying in-situ mechanical test stages: a Zeiss Xraida 520 and Bruker Skyscan 1172. The Zeiss can achieve higher resolution due to the utilization of objective lenses rather than relying strictly on geometric magnification. Therefore, the Zeiss Xradia 520 XCT system was used for all of the scans reported in this study. A Deben mechanical test stage is the accessory stage that is directly compatible with the Zeiss scanner; however, the large physical size of the test stage was problematic. X-ray intensity is proportional to the distance travelled between the source and detector in accordance with the inverse square law. Due to the large geometry of the Deben in-situ mechanical test stage, a large distance is required between the source and detector, which leads to low signal intensity and difficulties achieving high-resolution scans. Figure 2A shows a 10-mm distance between the X-ray source and sample and an 8-mm distance between the sample and detector, which are common distances for high-resolution (~1-µm voxel size) scans. Figure 2B, however, shows the large increase in the distances when the stage is incorporated, and the minimum distances are 63 and 35 mm between source to sample and sample to detector, respectively. This increase from 18 to 98 mm is significant. With the distance being over five times more, the resulting signal intensity at the same voltage applied would be less than 4% of the close distance.

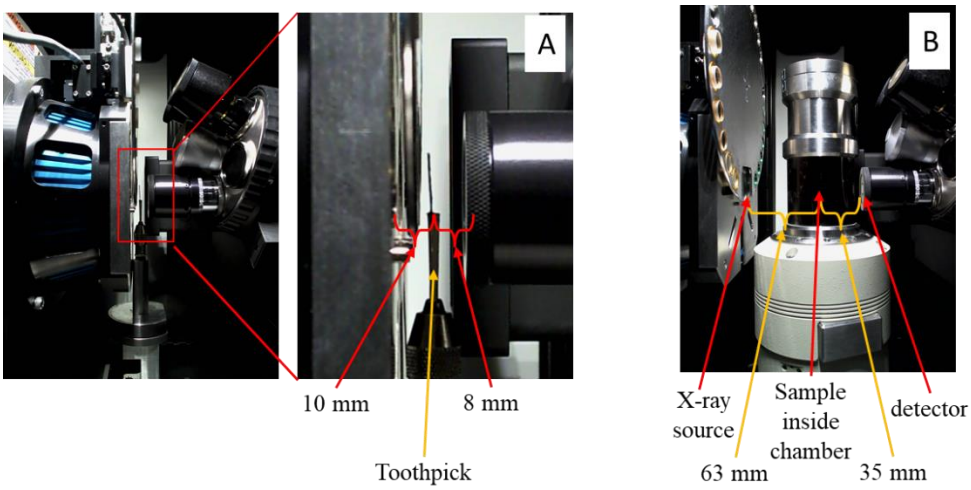

Fig. 2 A) Typical distances between the X-ray source, sample, and detector for high-resolution scans without a mechanical test stage, and B) minimum distances with the Deben mechanical test stage

The desired resolution would not be possible while incorporating the large mechanical test stage because the intensity was too low. To overcome this challenge, a smaller mechanical test stage that is an accessory stage for the Bruker Skyscan 1172 MicroCT was explored. This smaller stage, pictured in Fig. 3, shows the minimum spacings of 38 and 20 mm between source to sample and sample to detector. This total distance of 58 mm provided adequate signal intensity to achieve the desired resolution. Therefore, loading was applied in the Bruker XCT system and then transferred to the Zeiss XCT system for scanning.

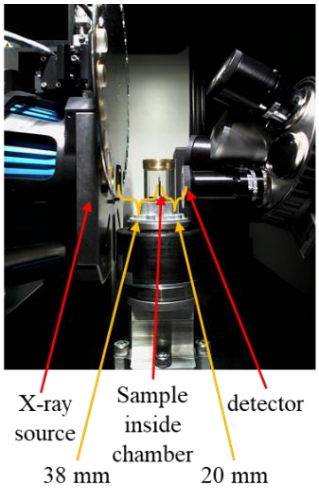

Fig. 3 Bruker Skyscan 1172 in-situ loading stage in the Zeiss Xradia 520 scanner, reducing the overall source-to-detector distance from 98 to 58 mm

After initial loading in the Bruker system, the in-situ stage was transferred to the Zeiss XCT for scanning. Scan settings of 60-kV voltage, 4-W power, 3201 projections, and 5-s exposure time were used and the resulting voxel size was 2.93 μm. The total scan time was 5.5 h.

Because the load cell was too high for the forces applied and the loading stage moved between two different XCT scanners, it was not possible to obtain quantitative loading results so subsequent stress versus strain curves could not be calculated. Instead, the tensile samples with and without the coating were loaded together to achieve the same displacements at both low and high strains for comparative analysis.

2.3 Quantitative Analysis

2.3.1 Volume Graphics

An important research question is whether there is preferential formation of the cavities on the larger glass spheres. If so, stricter requirements regarding the largest acceptable glass sphere sizes or a more tightly controlled sphere distribution might be necessary for particular applications. To help answer this question, Volume Graphics 3.0 was used to segment the glass spheres, conduct a volume analysis on them, and qualitatively compare the locations of the cavity formations and their respective glass sphere sizes.

2.3.2 CTAn Analysis

Bruker's CTAnalyzer (CTAn) software version 1.18.4.0 was used to generate 3-D models of each sample as well as segment and quantify the glass sphere sizes based on their volume. Additionally, the cavity frequency and sizes were also segmented and quantified. An image analysis task list was programmed that started with an automatic thresholding function to isolate and binarize the glass spheres. Despeckling functions were applied to eliminate excess noise, fill in the holes within the glass spheres, and remove partial spheres on the image borders. Next, erosion/dilation functions were applied to fill in some holes within the glass spheres that were open to the matrix, followed by a watershed segmentation function to separate touching glass spheres so multiple spheres would not be counted as one larger object. Once the images were properly corrected, a quantitative analysis was conducted that included 2-D, 3-D, and individual object analysis. Despeckling functions were used to isolate glass spheres between the ranges of 2000–4000, 4000–6000, 6000–8000, and greater than 8000 voxels for future 3-D model visualization of each subset.

The segmented glass sphere data was saved for later application. The original raw images were reloaded and a thresholding was applied to isolate the cavity phase. Some spheres had internal porosity that was the same contrast as the cavities of interest, which caused issues during segmentation. Therefore, segmented spheres that previously had their porosity filled in through the despeckling function were used to mask their porosity so the cavity segmentation would not include them. Utilizing bitwise operations, the cavities were successfully isolated from the internal sphere porosity, which provided much-more accurate results. The isolated cavities were then quantified using the 2-D, 3-D, and individual object analysis functions as well as the 3-D model function for visualization purposes.

2.3.3 MATLAB Image Segmentation and Analysis

A custom MATLAB code was written to further expand the quantitative analysis, specifically for differentiating between glass spheres with and without attached cavities. A similar image-processing pipeline to that of CTAn was applied to each physical sample's XCT image data set using built-in and customized MATLAB functions. The image-processing pipelines for both glass and cavity phases are summarized in Table 1.

Table 1. Processing steps for segmentation and correction of glass and cavity phases in MATLAB

Pipeline for glass phase	Pipeline for cavity phase
Fill holes	Intensity thresholding
2-D area filter	2-D area filter
2-D watershed	3-D rescale to micron
2-D convex hull generation	Major axis length filters
3-D rescale to micron	Object slice length filter
3-D watershed	Sphericity filter
Major axis length filters	Phase distance filter (only for plotting)
3-D volume filter	…
Edge filter	…

Upon pipeline completion, each cavity and glass phase's location and size were calculated and saved for future application. CTAn glass sphere and cavity sizes and locations were also imported into MATLAB for comparison to and validation of the MATLAB results. Additional calculations were performed within MATLAB to determine the number of attached cavities as well. A cavity was determined attached only if its phase distance, or the distance between associated glass and cavity centroids, was less than a given upper limit. All cavities that fell within this upper limit and their subsequent phase distances were saved for future analysis. Phase distance calculations were performed on both the MATLAB and CTAn results. Finally, to answer whether there is preferential formation of cavities on

larger glass spheres, a size comparison analysis was conducted between glass spheres with attached cavities and the entire glass sphere phase. Overlaid histogram distributions of the two glass sphere data sets for each physical sample were generated in an attempt to discover where cavities are more likely to form.

3. Results and Discussion

3.1 XCT Results

Representative XCT volume renderings are shown in Fig. 4 with and without a tensile load applied and using the software program CTVox. The glass spheres are the highest density phase and appear with the brightest contrast. The cavities are the darkest contrast above or below the glass spheres consistent with the direction of tensile load applied and indicated by the red arrows as shown in Fig. 4B.

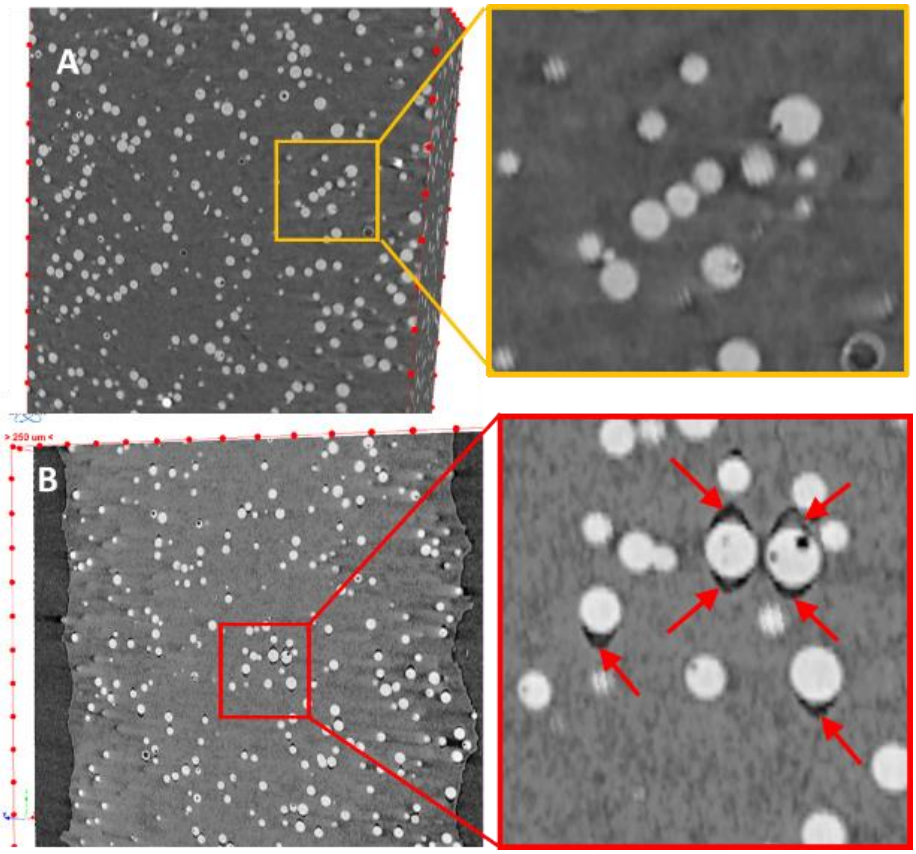

Fig. 4 A) Representative XCT images with no load applied (top) and B) scan with load applied showing cavities between the glass spheres and matrix, indicated by the red arrows (bottom); the spacing between red dots is 250 µm

3.2 Volume Graphics

Volume Graphics software was used to aid answering the question regarding preferential formation of cavities on larger glass spheres. Figure 5A shows the segmented cavities, Fig. 5B adds an additional segmentation of the cavities shown in red, Fig. 5C illustrates the volume analysis with the spheres colored according to size, and Fig. 5D combines the volume analysis with the cavities in red. Qualitatively, there did not appear to be a preferential formation of cavities on larger or smaller glass spheres. These results were somewhat counterintuitive, so there was an interest in exploring the relative sizes of the cavities and respective glass spheres through a more in-depth and quantitative analysis.

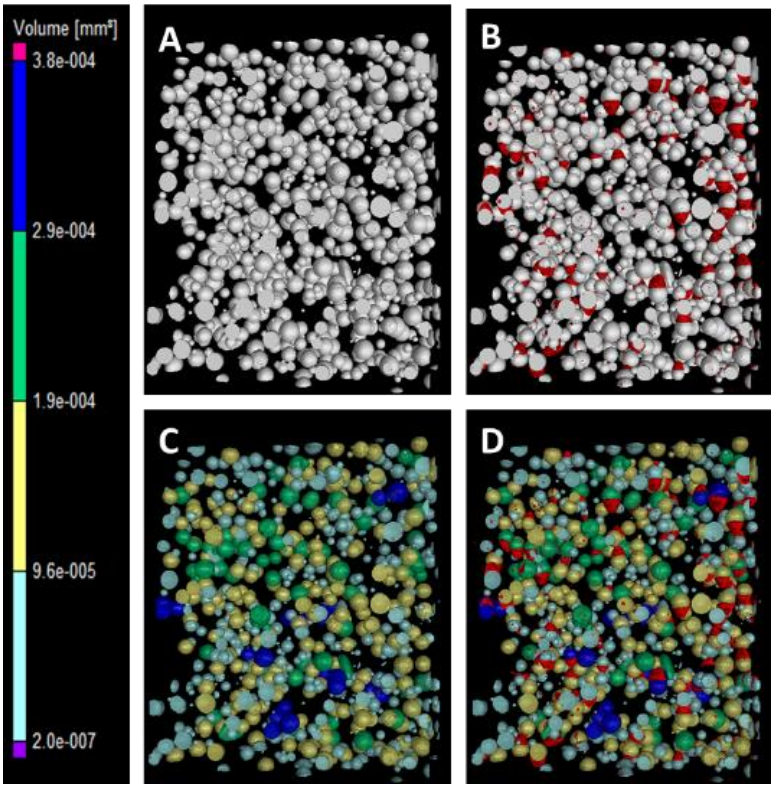

Fig. 5 A) Segmented spheres in white, B) segmented spheres (white) and segmented cavities (red), C) volumetric analysis of the glass spheres with colors corresponding to the scale on the left, and D) volumetric analysis and cavities (in red)

3.3 CTAn Analysis

Figures 6A and 6B show quantitative results for the cavity segmentation in CTAn. As expected, the low strains had fewer cavities and smaller volumes compared to the same samples loaded at a higher strain. Also unsurprisingly, the coated samples had fewer total cavities and smaller volumes compared to the uncoated samples at the same strains. Interestingly, the high strain coated had fewer separations than the

low strain uncoated but a higher average cavity size, demonstrating the effectiveness of the coating to reduce the formation of new cavities at higher strains and therefore improving the mechanical performance with regard to the strain to failure.

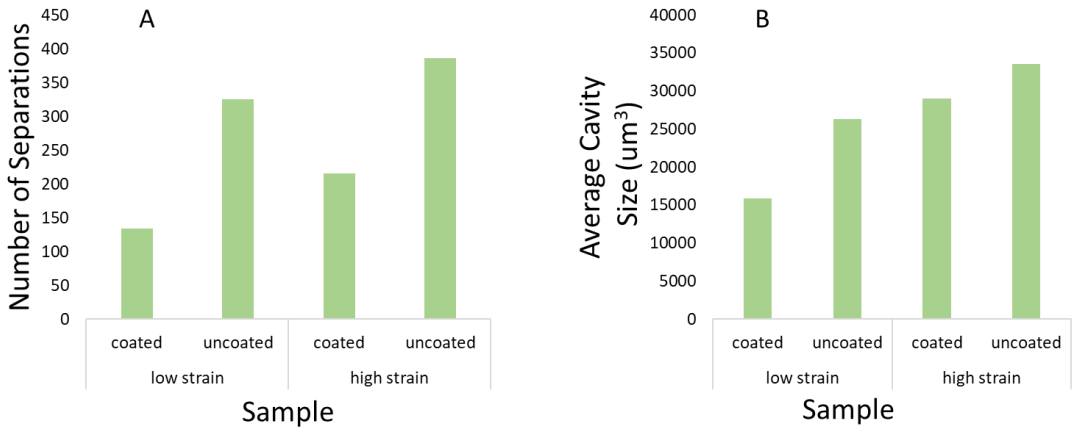

Fig. 6 Quantitative CTAn results of A) the total number of cavity separations B) the average size of the cavities

To visualize the cavities respective to varying glass sphere volumes, 3-D models were generated with different voxel size ranges. Figure 7A–D shows the glass spheres binned at varying size intervals and the models viewed in Bruker CTVol software version 2.3.1.0. Additionally, a 3-D model of the segmented cavities is shown in Fig. 7E.

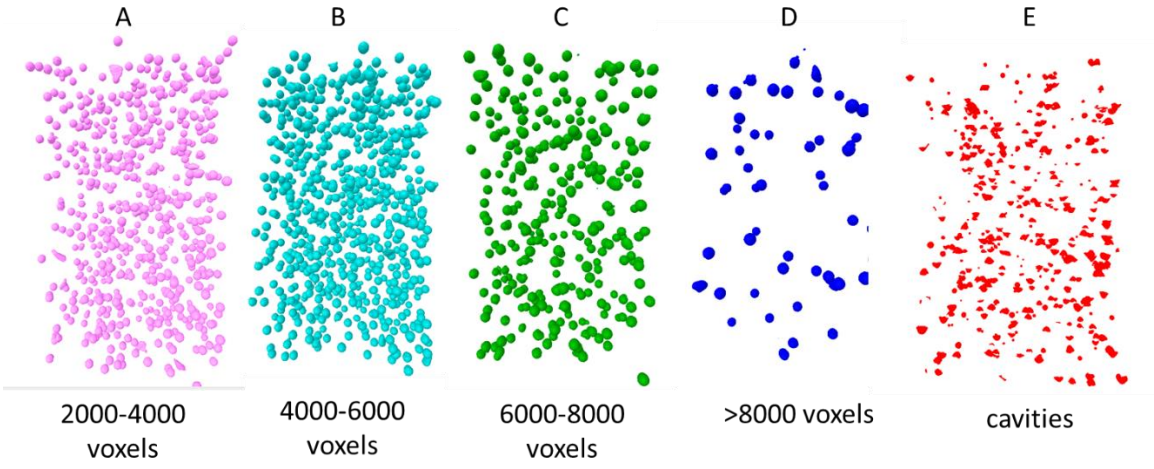

Fig. 7 Segmented glass spheres at varying size ranges (A–D) and cavities (E)

Combining all of the glass spheres' sizes as well as the cavities is shown in Fig. 8A. When looking closely within the volume, it is clear that cavities formed on all of the different glass sphere sizes and there was not preferential formation on larger

spheres, which is in agreement with the previous Volume Graphics visualizations. Unfortunately, there was not a straightforward method to isolate only the glass spheres with attached cavities apart from the glass spheres with no cavities in CTAn. This limits the depth of the analysis, particularly quantifying the relative distribution of the sphere distribution with the attached cavities to the overall distribution of the glass spheres (with and without the attached cavities). Therefore, further analysis through a customized MATLAB code was explored.

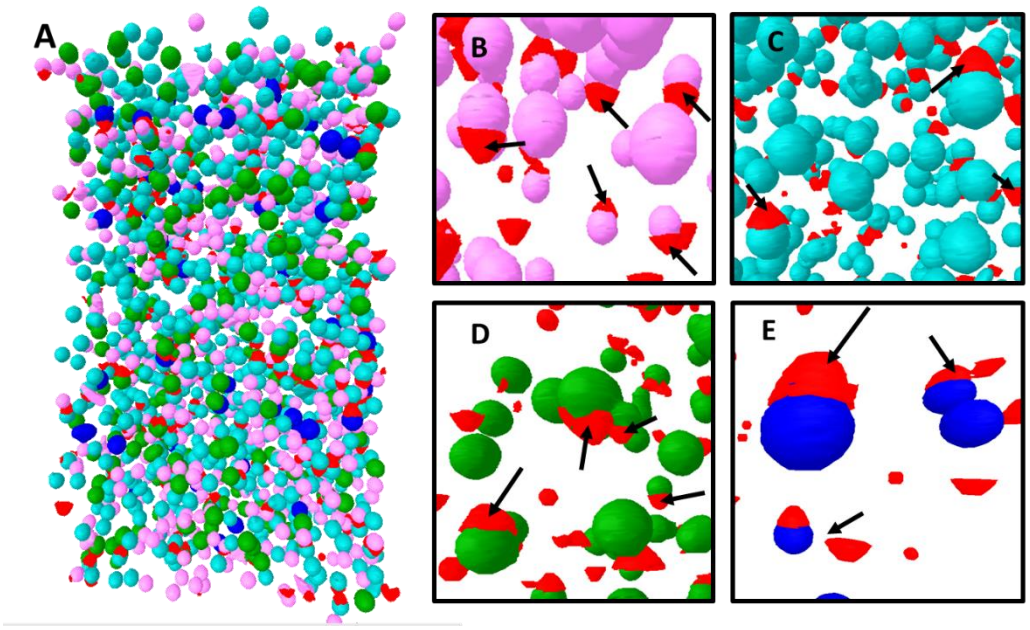

Fig. 8 A) All of the glass sphere size ranges and cavities; and B–E) isolated ranges and cavities demonstrate no preferential formation on particular glass sphere sizes

3.4 MATLAB

A comparison of the CTAn and MATLAB segmented centroids of both the glass and cavity phases is shown in Fig. 9. The difference between the two programs and by two different researchers was almost entirely less than 10 µm (Fig. 9A and 9B). Considering the voxel size was 2.93 µm, the centroids were only a few pixels between one another, which indicates very close agreement. Figure 9C shows an overlay of the glass centroids calculated by the CTAn software (in red) and the 3-D glass objects calculated by MATLAB (in blue, only showing the bottom half), visually confirming the quantitative results and suggesting there is close agreement between the two software programs.

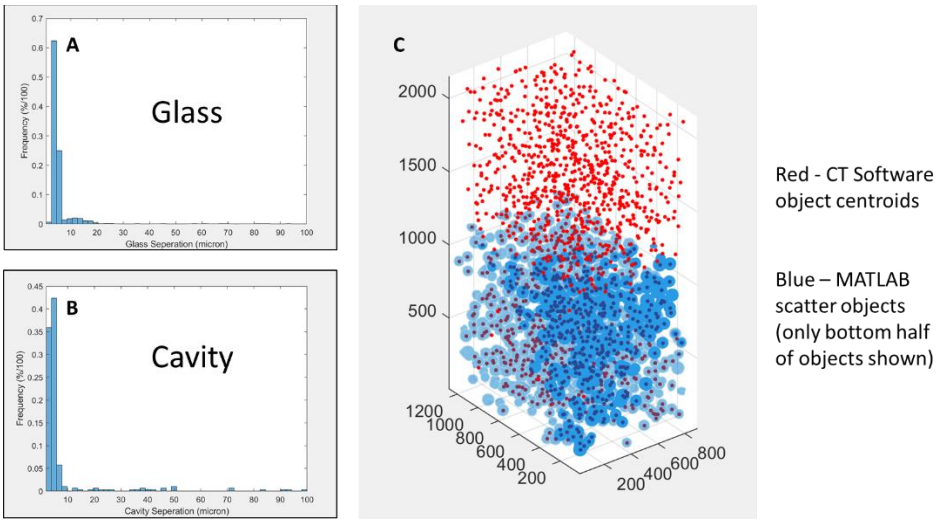

Fig. 9 Comparing MATLAB and CTAn centroids of glass spheres

Additional quantitative analysis showed a similar number of cavity separations (Fig. 10A) between CTAn and MATLAB. The average cavity size, however, was different between the two programs (Fig. 10B), which was likely due to differing levels of noise reduction filters (i.e., despeckling functions) or differences between watershed algorithms used to separate touching glass spheres.

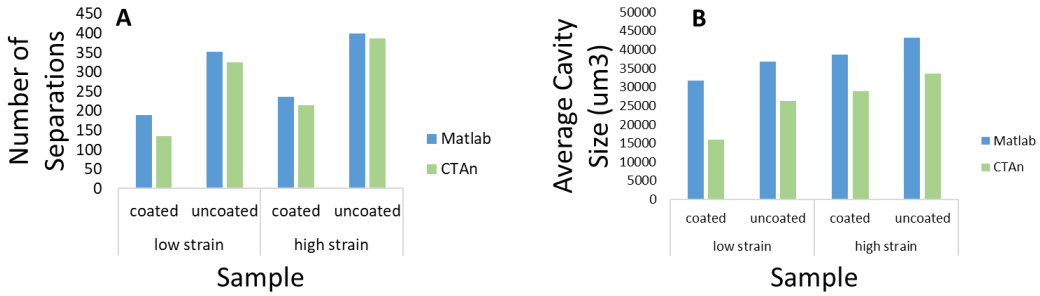

Fig. 10 Comparison between MATLAB and CTAn segmentations for A) number of cavity separations and B) average cavity size

A phase distance upper limit was established to determine whether any given glass sphere truly had an attached cavity. Figure 11 shows the phase distance, or cavity spacing, for segmentation through both software programs. A majority of the phase distances were between 20–40 µm for both MATLAB and CTAn results. The larger spacings were on the order of 60 µm, therefore an attached cavity was defined as having a phase distance of 70 µm or less.

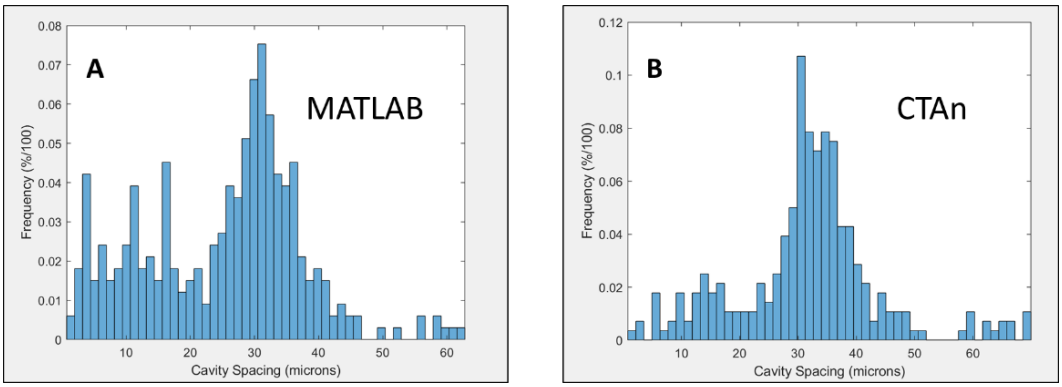

Fig. 11 Cavity spacing (the distance between the cavity centroid and glass sphere centroid) for A) MATLAB segmentation and B) CTAn segmentation

To quantitatively discern any preferential formation on larger glass spheres, the glass sphere distributions needed to be compared between those with attached cavities and all of the glass spheres, as illustrated in Fig. 12. A shift in the histograms with the glass spheres of only the attached cavities being larger would indicate preferential formation on the larger sizes, and similar histogram distributions would indicate no preferential formation. Therefore, histograms were generated for each sample with and without the attached cavities, and the results are shown in Fig. 13. The coated glass spheres had very similar histogram distributions at both high (Fig. 13A) and low (Fig. 13C) strains. Additionally, the distributions of the glass spheres with the attached cavities (shown in blue) are very similar when comparing the coated and uncoated data sets.

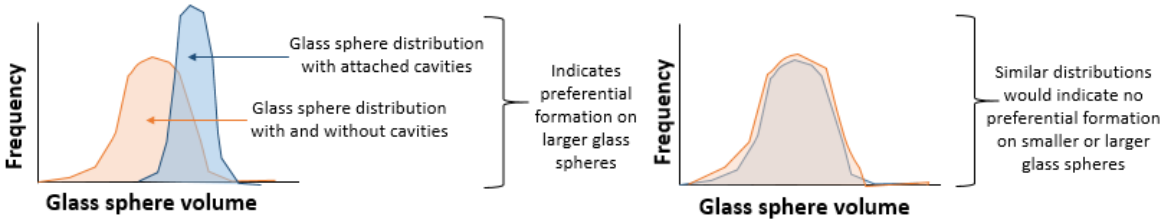

Fig. 12 Histograms of glass spheres with attached cavities compared to all of the glass spheres. A) a shift in the histogram of the glass spheres with attached cavities indicates preferential formation on larger glass sphere sizes and B) similar histogram distributions indicate no preferential formation.

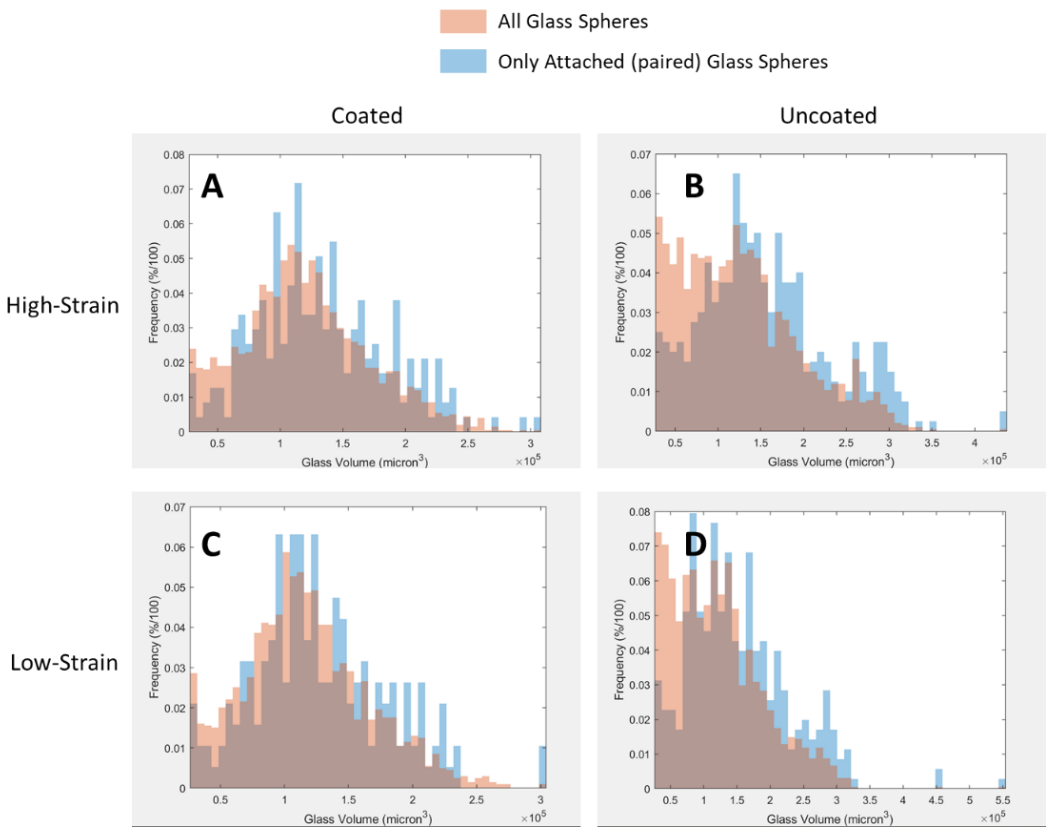

Fig. 13 Distributions of all of the segmented glass spheres and the segmented glass spheres of only those with attached (paired) cavities for A) high strain coated, B) high strain uncoated, C) low strain coated, and D) low strain uncoated

For the uncoated samples, there might be a slight preferential formation on the larger glass spheres, which may be due to differences in the sphere size distributions of the (all) glass sphere condition. Interestingly, the distribution of the uncoated (all) glass spheres has a higher frequency of smaller glass spheres compared to the uncoated glass spheres of only those with attached cavities. One explanation is that the coating process might be eliminating the smallest glass spheres (~0.5×10^5 µm^3), which would explain differences between Figs. 13A and 13B and Figs. 13C and 13D for the all-glass sphere condition. This was further explored through particle size analysis on the same batch of glass spheres in both coated and uncoated conditions. It was found that there was indeed a slightly larger particle size distribution for the coated spheres compared to the uncoated, and the difference was more pronounced at the smallest size. Table 2 summarizes the average diameter of the glass spheres at the 10th, 50th, and 90th percentiles. The 10th percentile had a difference of approximately 8 µm between the coated and uncoated, whereas the 50th and 90th percentiles were much closer at 3–4 µm. Additionally, the equivalent sphere diameter for the 0.5×10^5 µm^3 volume quantified through the XCT

measurements is 45.7 µm, which agrees very well with the 10th percentile measurements for the uncoated spheres.

Table 2. Glass sphere diameter for coated and uncoated particles at the 10th, 50th, and 90th percentiles

Percentile	Glass sphere diameter (µm)	
	Coated	**Uncoated**
10th	57.02	49.29
50th	68.31	65.17
90th	85.15	81.92

The results in Fig. 12 confirm what was seen qualitatively through both Volume Graphics and CTAn visualizations. There does not appear to be any preferential formation for the larger glass sphere sizes for the coated samples, otherwise there would be a noticeable shift in the histograms with the glass spheres of only the attached cavities being larger in volume. This is an important finding because it indicates the binder interface failure is not necessarily dependent on the glass sphere volume and therefore the distribution of the particle additives would not need to be as tightly controlled.

4. Conclusions

A technique that demonstrates the feasibility of laboratory-scale XCT experiments for full 3-D imaging of cavity formation and growth during in-situ loading has been detailed in this report. The number of cavities and cavity sizes can readily be quantified. More advanced techniques can be used to separate the glass spheres with attached cavities from all of the other glass spheres to draw conclusions regarding preferential formation based on particle size. While this study did not show any preferential formation based upon particle size, it is important to note that different materials, surface-treatment coatings, ranges of particle sizes, particle shapes, or volume fractions of solids loadings may have very different results.

5. Future Work

Additional experiments are planned at the Cornell High Energy Synchrotron Source (CHESS) through the Materials Solutions Network at CHESS. With the synchrotron having a monochromatic beam and a much higher X-ray intensity flux, experiments are conducted in a fraction of the time as compared to the laboratory XCT scanner. Preliminary experiments showed similar results in a 6-min scan compared to the 5.5-h scan times conducted for the results in this report. This time

savings will allow the exploration of various chemistries, solids loadings, strain increments, and glass sphere sizes. Other future work possibilities include volumetric image correlation for obtaining 3-D strain information as well as generating meshes for models and simulations.

6. References

1. Jerabek M, Major Z, Renne K, Móczó J, Pukánszky B, Lang RW. Filler/matrix-debonding and micro-mechanisms of deformation in particulate filled polypropylene composites under tension. Polymer. 2010;51(9):2040–2048.

2. Lee J, Yee AF. Fracture of glass bead/epoxy composites: on micro-mechanical deformations. Polymer. 2000;41(23):8363–8373.

3. Liang JZ, Li RKY, Tjong SC. Morphology and tensile properties of glass bead filled low density polyethylene composites: material properties. Polymer Testing. 1999;16(6):529–548.

4. Yan W, Lin RJT, Bhattacharyya D. Particulate reinforced rotationally moulded polyethylene composites – mixing methods and mechanical properties. Compos Sci Tech. 2006;66(13):2080–2088.

5. Mousa AA. The effects of content and surface modification of filler on the mechanical properties of selective laser sintered Polyamide12 composites. Jordan J Mech Ind Eng. 2014;8(5):265–274.

6. Kawaguchi T, Pearson RA. The effect of particle–matrix adhesion on the mechanical behavior of glass filled epoxies. Part 2. A study on fracture toughness. Polymer. 2003;44(15):4239–4247.

7. Thio YS, Argo AS, Cohen RE. Role of interfacial adhesion strength on toughening polypropylene with rigid particles. Polymer. 2004;45(10):3139–3147.

8. Babout L, Maire E, Buffiere JY, Fougeres R. Characterization by X-ray computed tomography of decohesion, porosity growth and coalescence in model metal matrix composites. Acta Materialia. 2001;29(11):2055–2063.

9. Buffiere JY, Maire E, Adiren J, Masse JP, Boller E. In situ experiments with X-ray tomography: an attractive tool for experimental mechanics. Exper Mech. 2010;50:289–305.

List of Symbols, Abbreviations, and Acronyms

2-D	two-dimensional
3-D	three-dimensional
ARL	Army Research Laboratory
CHESS	Cornell High Energy Synchrotron Source
CTAn	CTAnalyzer
CTVol	software program for visualizing 3-D models
CTVox	software program for 3-D volume renderings
DEVCOM	US Army Combat Capabilities Development Command
IBA	isobornyl acrylate
UA	urethane acrylate
UV	ultraviolet
XCT	X-ray micro-computed tomography

1 (PDF) DEFENSE TECHNICAL INFORMATION CTR
DTIC OCA

1 (PDF) DEVCOM ARL
FCDD RLD DCI
TECH LIB

15 (PDF) DEVCOM ARL
FCDD RLW D
J ROBINETTE
FCDD RLW M
E CHIN
FCDD RLW MB
JM SIETINS
B LOVE
J SUN
T WALTER
W GREEN
FCDD RLW MD
A KUDZAL
I MCANINCH
C MOCK
FCDD RLW TB
CA GUNNARSSON
S ALEXANDER
A BROWN
FCDD RLW WB
D VANOOSTEN
J SADLER